
This is an electronic reprint of the original article.
This reprint may differ from the original in pagination and typographic detail.

Qu, Zengcai; Ranta, Mikaela; Hinkkanen, Marko; Luomi, Jorma

Loss-minimizing flux level control of induction motor drives

Published in:
IEEE Transactions on Industry Applications

DOI:
[10.1109/TIA.2012.2190818](https://doi.org/10.1109/TIA.2012.2190818)

Published: 15/05/2012

Document Version
Peer reviewed version

Please cite the original version:
Qu, Z., Ranta, M., Hinkkanen, M., & Luomi, J. (2012). Loss-minimizing flux level control of induction motor drives. *IEEE Transactions on Industry Applications*, 48(3), 952-961. <https://doi.org/10.1109/TIA.2012.2190818>

This material is protected by copyright and other intellectual property rights, and duplication or sale of all or part of any of the repository collections is not permitted, except that material may be duplicated by you for your research use or educational purposes in electronic or print form. You must obtain permission for any other use. Electronic or print copies may not be offered, whether for sale or otherwise to anyone who is not an authorised user.

Loss-Minimizing Flux Level Control of Induction Motor Drives

Zengcai Qu, Mikaela Ranta, Marko Hinkkanen, *Member, IEEE*, and Jorma Luomi, *Member, IEEE*

Abstract—The paper applies a dynamic space-vector model to loss-minimizing control in induction motor drives. The induction motor model, which takes hysteresis losses and eddy-current losses as well as the magnetic saturation into account, improves the flux estimation and rotor-flux-oriented control. Based on the corresponding steady-state loss function, a method is proposed for solving the loss-minimizing flux reference at each sampling period. A flux controller augmented with a voltage feedback algorithm is applied for improving the dynamic operation and field weakening. Both the steady-state and dynamic performance of the proposed method is investigated using laboratory experiments with a 2.2-kW induction motor drive. The method improves the accuracy of the loss minimization and torque production, it does not require excessive computational resources, and it shows fast convergence to the optimum flux level.

Index Terms—Control, core losses, efficiency optimization, field weakening, induction machine.

I. INTRODUCTION

In variable-speed induction motor (IM) drives, the core losses and the resistive losses depend on the flux level. A large number of loss minimization strategies have been developed for adjusting the flux level according to the motor load and speed. These loss minimization control techniques have been reviewed, e.g., in [1], [2]. Principally, the methods can be divided into two categories: online search controllers and loss-model-based controllers. Online search controllers measure the input power and iteratively change the flux level until the input power minimum is detected. They do not rely on motor parameters, but their convergence tends to be slow and they may cause flux and torque pulsations. Loss-model-based controllers use a functional loss model for evaluating the optimum flux level [3], [4], [5]. They are normally faster than online search methods but sensitive to parameter variations. However, loss-model-based controllers are well suited to IM drives where vector control is used and motor parameters are needed for the control.

Various loss functions have been used for describing the IM losses [2]. The resistive losses and core losses of the motor are commonly included in the loss model. Usually, the core losses are assumed to be proportional to the square of the frequency;

This work was supported by the Academy of Finland and ABB Oy. The preliminary version of this paper was presented at the IEEE International Electric Machines & Drives Conference (IEMDC), Niagara Falls, Canada, May 15–18, 2011.

Z. Qu, M. Ranta, and M. Hinkkanen are with Aalto University, Department of Electrical Engineering, P.O. Box 13000, FI-00076 Aalto, Espoo, Finland (e-mail: zengcai.qu@aalto.fi; mikaela.ranta@aalto.fi; marko.hinkkanen@aalto.fi).

J. Luomi, deceased, was with Aalto University, Department of Electrical Engineering, P.O. Box 13000, FI-00076 Aalto, Espoo, Finland.

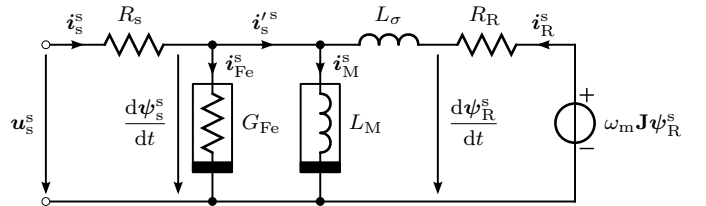


Fig. 1. Dynamic Γ model of the IM in stator coordinates. The voltage across the core-loss conductance G_{Fe} is $u_{Fe}^s = d\psi_s^s/dt$.

this behaviour corresponds to eddy-current losses. It is also possible to include both eddy-current losses and hysteresis losses in the loss model [6], [7]. If the loss model is sufficiently simple, the optimum flux level can be solved analytically. For more complicated loss models, it is possible to determine the optimum flux level iteratively [1].

In this paper, the dynamic space-vector model proposed for IMs in [8] is applied to loss-minimizing control. The model includes both hysteresis losses and eddy-current losses as well as the magnetic saturation. The core losses and the magnetic saturation are also taken into account in the flux estimation and rotor-flux-oriented control. Based on the corresponding steady-state loss function, a method is proposed for solving the loss-minimizing flux reference at each sampling period. In order to improve the dynamic operation of the drive, a proportional flux controller is applied. The flux controller is also augmented with a voltage-feedback field-weakening algorithm. Both the steady-state performance and the dynamic performance of the proposed method are investigated using laboratory experiments with a 2.2-kW IM drive.

II. Γ MODEL

Real-valued space vectors will be used; for example, the stator-flux vector is $\psi_s = [\psi_{sd}, \psi_{sq}]^T$ and its magnitude is denoted by

$$\psi_s = \|\psi_s\| = \sqrt{\psi_{sd}^2 + \psi_{sq}^2} \quad (1)$$

The space vectors in stator coordinates are denoted by the superscript s and no superscript is used for vectors in synchronous coordinates. The identity matrix is $\mathbf{I} = \begin{bmatrix} 1 & 0 \\ 0 & 1 \end{bmatrix}$ and the orthogonal rotation matrix is $\mathbf{J} = \begin{bmatrix} 0 & -1 \\ 1 & 0 \end{bmatrix}$. Per-unit quantities will be used.

A. Voltage and Flux Equations

Fig. 1 shows the dynamic Γ model of the IM in stator coordinates [9]. In synchronous coordinates rotating at ω_s , the

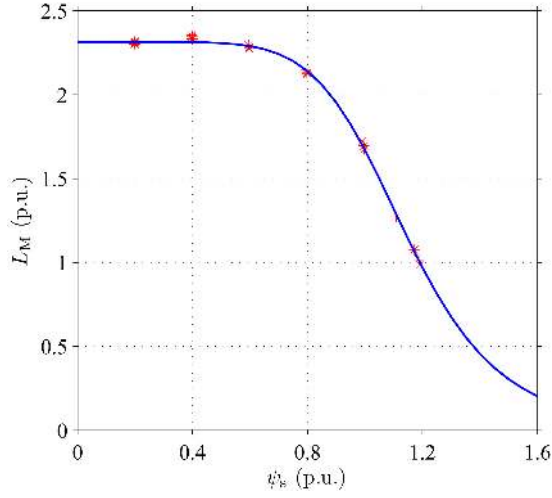


Fig. 2. Stator inductance (5) as a function of the stator flux for $L_u = 2.31$ p.u., $\beta = 0.87$ p.u. and $S = 7$. Markers show the measured inductance values from no-load tests (different stator frequencies were applied at each flux level).

IM model can be described by the voltage equations

$$\frac{d\psi_s}{dt} = \mathbf{u}_s - R_s \mathbf{i}_s - \omega_s \mathbf{J} \psi_s \quad (2a)$$

$$\frac{d\psi_R}{dt} = -R_R \mathbf{i}_R - \omega_r \mathbf{J} \psi_R \quad (2b)$$

where the stator voltage vector is denoted by \mathbf{u}_s , the stator current vector by \mathbf{i}_s , and the stator resistance by R_s . The rotor current vector is \mathbf{i}_R and the rotor resistance is R_R . The angular slip frequency $\omega_r = \omega_s - \omega_m$, where ω_m is the electrical angular speed of the rotor. The stator and rotor flux linkages are given by

$$\psi_s = L_M(\mathbf{i}'_s + \mathbf{i}_R) \quad (3a)$$

$$\psi_R = \psi_s + L_\sigma \mathbf{i}_R \quad (3b)$$

respectively, where $\mathbf{i}'_s = \mathbf{i}_s - \mathbf{i}_{Fe}$, the stator inductance is L_M , and the leakage inductance is L_σ . The current of the core-loss conductance G_{Fe} is \mathbf{i}_{Fe} , and the voltage across the core-loss conductance is

$$\mathbf{u}_{Fe} = \mathbf{u}_s - R_s \mathbf{i}_s \quad (4)$$

B. Magnetic Saturation

The stator inductance and the leakage inductance depend on the flux linkages (or the currents) due to the magnetic saturation [10]. If the loss-minimizing flux level control is to be applied, the magnetic-saturation effects should be modeled and taken into account in the control algorithms.

In the case of the Γ model, modeling the stator inductance L_M as a function of the stator flux typically suffices.¹ The leakage inductance L_σ is assumed to be constant and the stator inductance is modeled by a simple power function [1], [12]:

$$L_M(\psi_s) = \frac{L_u}{1 + (\beta \psi_s)^S} \quad (5)$$

¹For achieving the same accuracy, more complex saturation models would be needed in the case of the inverse- Γ model [11]. The transformation between the inverse- Γ model and the Γ model is given in the Appendix.

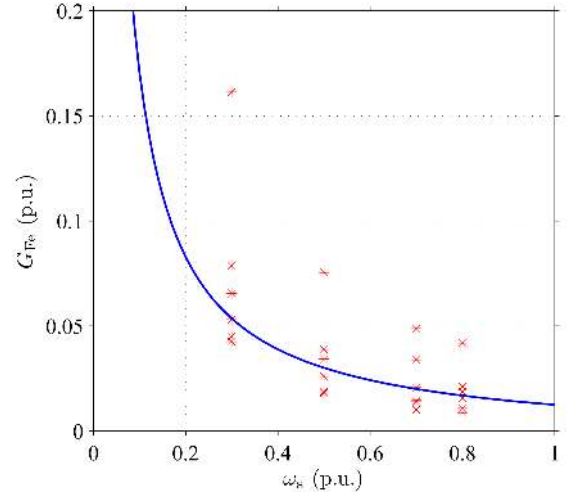


Fig. 3. Steady-state core-loss conductance (7) as a function of stator frequency for $\Lambda_{Hy} = 0.015$ p.u. and $G_{Ft} = 0$ p.u. Markers show the measured conductance values from no-load tests (different flux levels were applied at each stator frequency).

where L_u is the unsaturated inductance, and S and β are nonnegative constants. These parameters can be identified using series of no-load tests at different voltage levels. Fig. 2 shows the stator inductance as a function of the stator flux.

C. Core-Loss Conductance

The core losses can be divided into two parts: hysteresis losses and classical eddy current losses. The hysteresis losses are proportional to the frequency, while the eddy current losses are proportional to the square of the frequency [13]. In steady state, the stator core losses are classically modeled as a function of the stator angular frequency ω_s and the stator-flux magnitude ψ_s ,

$$P_{Fe} = \underbrace{\Lambda_{Hy} |\omega_s| \psi_s^2}_{P_{Hy}} + \underbrace{G_{Ft} \omega_s^2 \psi_s^2}_{P_{Ft}} \quad (6)$$

where the first term corresponds to the hysteresis losses P_{Hy} and the second term corresponds to the eddy-current losses P_{Ft} . The constants Λ_{Hy} and G_{Ft} determine the ratio between the loss components at a given stator flux and angular frequency. The steady-state core-loss conductance corresponding to (6) is

$$G_{Fe}(\omega_s) = \frac{\Lambda_{Hy}}{|\omega_s|} + G_{Ft} \quad (7)$$

which is illustrated in Fig. 3. The parameters Λ_{Hy} and G_{Ft} can be identified using series of no-load tests at different stator frequencies.

The steady-state model (7) cannot be directly used in dynamic models since the angular frequency ω_s is irrelevant in transients and in the case of non-sinusoidal waveforms. In the following, a nonlinear core-loss conductance [8]

$$G_{Fe}(u_{Fe}, \psi_s) = \Lambda_{Hy} \frac{\psi_s}{u_{Fe}} + G_{Ft} \quad (8)$$

is applied in the dynamic Γ model. The conductance depends on the magnitude of the instantaneous voltage across it and the

magnitude of the instantaneous stator flux. The instantaneous core losses become $p_{\text{Fe}} = \Lambda_{\text{Hy}} u_{\text{Fe}} \psi_s + G_{\text{Ft}} u_{\text{Fe}}^2$, which equals (6) in steady state.

D. Loss Function in Steady State

The power balance of the IM model is given by

$$\mathbf{i}_s^T \mathbf{u}_s = R_s i_s^2 + R_R i_R^2 + p_{\text{Fe}} + \frac{dW_f}{dt} + T_e \omega_m \quad (9)$$

The electromagnetic torque is

$$T_e = \mathbf{i}_s^T \mathbf{J} \psi_s \quad (10)$$

and the rate of change of the magnetic energy is

$$\frac{dW_f}{dt} = \mathbf{i}_s^T \frac{d\psi_s}{dt} + \mathbf{i}_R^T \frac{d\psi_R}{dt} = i_M \frac{d\psi_s}{dt} + i_R \frac{d\psi_R}{dt} \quad (11)$$

In steady state, the power fed into the stator is

$$P_s = \mathbf{i}_s^T \mathbf{u}_s = P_{\text{loss}} + T_e \omega_m \quad (12)$$

where the total losses are

$$P_{\text{loss}} = R_s i_s^2 + R_R i_R^2 + (\Lambda_{\text{Hy}} |\omega_s| + G_{\text{Ft}} \omega_s^2) \psi_s^2 \quad (13)$$

The first term corresponds to the stator resistive losses, the second term to the rotor resistive losses, and the last term to the core losses.

For searching the loss-minimizing rotor-flux level, the loss function (13) will be formulated as a function of T_e , ω_m , and ψ_R in the following. Based on (2b) and (10), the slip angular frequency can be expressed as

$$\omega_r = \frac{R_R T_e}{\psi_R^2} \quad (14)$$

and the stator angular frequency is $\omega_s = \omega_m + \omega_r$. The rotor current can be solved from (2b) as

$$\mathbf{i}_R = -\frac{\omega_r \mathbf{J} \psi_R}{R_R} \quad (15)$$

The stator flux is obtained based on (3b) and (15) as

$$\psi_s = \left(\mathbf{I} + \frac{\omega_r L_\sigma}{R_R} \mathbf{J} \right) \psi_R \quad (16)$$

The magnetizing current is $i_M = \psi_s / L_M$ and the core-loss current is

$$\mathbf{i}_{\text{Fe}} = [\Lambda_{\text{Hy}} \text{sign}(\omega_s) + G_{\text{Ft}} \omega_s] \mathbf{J} \psi_s \quad (17)$$

Finally, the stator current is

$$\mathbf{i}_s = \mathbf{i}_{\text{Fe}} + \mathbf{i}_M - \mathbf{i}_R \quad (18)$$

Using (14)–(18), the losses in (13) can be expressed as a function of T_e , ω_m , and ψ_R . If the loss-minimizing flux magnitude is to be searched for a given operating point, T_e and ω_m can be considered as constant parameters.

Fig. 4 illustrates the loss-minimizing rotor flux as a function of the torque for a 2.2-kW IM. These flux values are found by numerically minimizing the loss function in (13). It can be seen that the loss-minimizing flux decreases strongly with the decreasing torque at torque levels below the rated torque. On the other hand, the loss-minimizing flux increases only moderately with the increasing torque at torque levels above the rated torque (due to the magnetic saturation). The loss-minimizing flux depends only slightly on the speed since the resistive losses are dominating in the example IM.

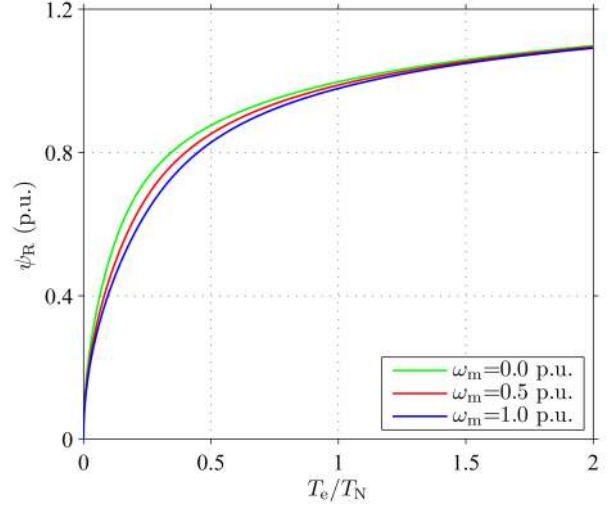


Fig. 4. Loss-minimizing rotor flux as a function of the torque at different speeds. The optimal flux is obtained by minimizing (13). The parameters of a 2.2-kW IM given in Table III were used.

III. CONTROL SCHEME

The speed-sensorless rotor-flux-oriented control system—augmented with the loss-minimizing flux level control—is shown in Fig. 5. The control system is based on the Γ model shown in Fig. 1, and it is implemented in estimated rotor-flux coordinates. The vector components in these coordinates will be marked by the subscripts d and q.

A. Flux Observer With Core-Loss Compensation

An inherently sensorless reduced-order rotor-flux observer is applied [14], [15], [16]. The observer is based on the voltage model, which is corrected by a current-model-based prediction error. More specifically, the error term is formulated using the component of the back electromotive force (EMF) induced by the rotor flux in the direction of the rotor-flux estimate. In this direction, the back EMF component computed from the current model does not depend on the speed estimate. The observer is implemented in estimated rotor-flux coordinates.

The observer is equal to [16] with two exceptions: (i) the observer is modified so that the parameters and variables correspond to those of the Γ model, which makes it easier to model the magnetic saturation and to incorporate the loss-minimizing method in the control system; (ii) the effect of the core losses is included in the observer. For clarity, the observer and these modifications are briefly described in the following.

In the observer, the stator inductance is obtained using the function $L_M(\hat{\psi}_s)$ defined in (5), where, naturally, the estimated stator-flux magnitude has to be applied. Similarly, the core-loss conductance is obtained using the function $G_{\text{Fe}}(\hat{u}_{\text{Fe}}, \hat{\psi}_s)$ defined in (8), where the magnitude of the voltage across the conductance is $\hat{u}_{\text{Fe}} = \|\mathbf{u}_s - \hat{R}_s \mathbf{i}_s\|$ and \hat{R}_s is the stator-resistance estimate. Furthermore, the magnetic coupling factor

$$\gamma(\hat{\psi}_s) = \frac{L_M(\hat{\psi}_s)}{L_M(\hat{\psi}_s) + L_\sigma} = \frac{L_u}{L_u + L_\sigma + L_\sigma(\beta \hat{\psi}_s)^S} \quad (19)$$

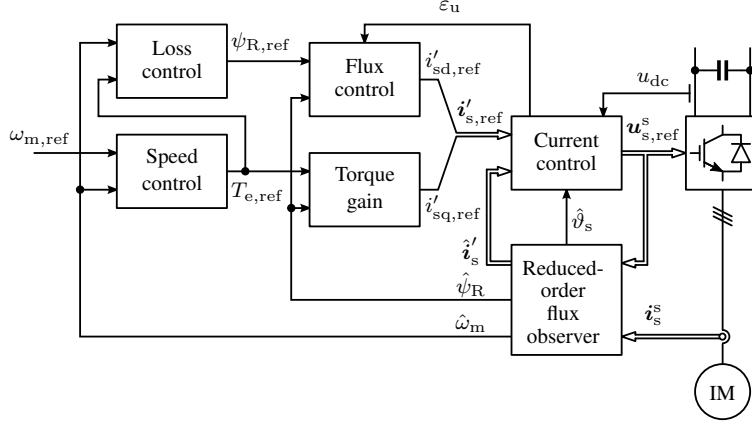


Fig. 5. Speed-sensorless rotor-flux-oriented control system. The observer provides the parameter estimates (\hat{R}_s , R_R , L_σ , and L_M) to other blocks, but, for clarity, these signals are not shown.

is applied. To simplify notation, the arguments of the functions L_M , G_{Fe} , and γ will be omitted in the following equations.

In order to take the core losses into account, the current i'_s going into the magnetic circuit is estimated as

$$\hat{i}'_s = i_s - G_{Fe}(u_s - \hat{R}_s i_s) \quad (20)$$

The estimates for the rotor-flux magnitude and position are obtained from

$$\frac{d\hat{\psi}_R}{dt} = e_d + g_1(\hat{e}_d - e_d) \quad (21a)$$

$$\frac{d\hat{\vartheta}_s}{dt} = \frac{e_q + g_2(\hat{e}_d - e_d)}{\hat{\psi}_R} = \hat{\omega}_s \quad (21b)$$

where the observer gains g_1 and g_2 equal the gains in [16]. The components of the back EMF induced by the rotor flux are calculated from the stator side as

$$e_d = \frac{1}{\gamma}(u_{sd} - \hat{R}_s i_{sd}) - L_\sigma \frac{d\hat{i}'_{sd}}{dt} + \hat{\omega}_s L_\sigma \hat{i}'_{sq} \quad (22a)$$

$$e_q = \frac{1}{\gamma}(u_{sq} - \hat{R}_s i_{sq}) - L_\sigma \frac{d\hat{i}'_{sq}}{dt} - \hat{\omega}_s L_\sigma \hat{i}'_{sd} \quad (22b)$$

The d component of the back-EMF estimate can be calculated from the rotor side as

$$\hat{e}_d = \gamma R_R \left(\hat{i}'_{sd} - \frac{\hat{\psi}_R}{L_M} \right) \quad (23)$$

Proper selection of the observer gains g_1 and g_2 is crucial, particularly for low-speed operation. It is worth noticing that the observer (21) would reduce to the pure voltage model (which cannot be used in practice) if $g_1 = g_2 = 0$ were used.

The estimate $\hat{\psi}_s$ for the stator-flux magnitude is needed for the functions G_{Fe} , L_M , and γ . This estimate depends on the rotor-flux estimate $\hat{\psi}_R$ and the current components according to

$$\hat{\psi}_s = \gamma \sqrt{(\hat{\psi}_R + L_\sigma \hat{i}'_{sd})^2 + (L_\sigma \hat{i}'_{sq})^2} = f(\hat{\psi}_s) \quad (24)$$

This nonlinear function cannot be explicitly solved. To circumvent this problem, the value of $\hat{\psi}_s$ from the previous time step is applied on the right-hand side of (24) in the

discrete-time implementation, i.e. $\hat{\psi}_{s,k+1} = f(\hat{\psi}_{s,k})$ where k is the time-step index. This computationally efficient method can be seen as the fixed-point iteration.²

The rotor-speed estimate is computed by embedding the slip relation in a low-pass filter

$$\frac{d\hat{\omega}_m}{dt} = \alpha_o \left(\hat{\omega}_s - \frac{\gamma R_R \hat{i}'_{sq}}{\hat{\psi}_R} - \hat{\omega}_m \right) \quad (25)$$

where α_o is the filter bandwidth. In order to tackle the effects of temperature variations, the stator-resistance adaptation law

$$\frac{d\hat{R}_s}{dt} = k_R \gamma (\hat{e}_d - e_d) \quad (26)$$

is applied, where the gain k_R equals the gain in [16]. The adaptation is disabled in the vicinity of no-load operation and at higher stator frequencies due to poor signal-to-noise ratio.

B. Loss-Minimizing Flux Reference

The total losses (13) should be minimized while the electromagnetic torque and the rotor speed should be controlled to their desired values. In a fashion similar to (13)–(18), the estimated total losses can be expressed as a function of the estimated rotor speed $\hat{\omega}_m$, the electromagnetic torque reference $T_{e,ref}$, and the (unfiltered) rotor flux reference $\psi_{R,ref}^*$. Since the loss-minimizing flux magnitude is to be determined for a given operating point, $\hat{\omega}_m$ and $T_{e,ref}$ are known, and thus the loss minimization law can be expressed as

$$\psi_{R,ref}^* = \arg \min_{\psi_R \in [\psi_{R,min}, \psi_{R,max}]} \{ \hat{P}_{loss}(\psi_R) \} \quad (27)$$

The minimum point of the loss function (13) can be very effectively found by means of a one-dimensional search method. At each sampling period, the golden section method is applied to search the loss-minimizing flux reference.

²The fixed-point iteration converges if $|df(\hat{\psi}_s)/d\hat{\psi}_s| < 1$, leading to the condition $L_u L_\sigma S(\beta \hat{\psi}_s)^S < \gamma [L_u + L_\sigma + L_\sigma (\beta \hat{\psi}_s)^S]^2$ if the effect of the core-loss compensation is omitted in (24). This condition is fulfilled for any realistic parametrizations of L_u , β , S , and L_σ . The nonlinear equation (24) could be avoided by changing the state variables of the observer, but the observer equations would become much more complex in that case.

Additionally, the calculated optimal rotor flux $\psi_{R,\text{ref}}^*$ is low-pass filtered as

$$\frac{d\psi_{R,\text{ref}}}{dt} = \alpha_{\text{lpf}} (\psi_{R,\text{ref}}^* - \psi_{R,\text{ref}}) \quad (28)$$

where $\psi_{R,\text{ref}}$ is the filtered flux reference and α_{lpf} is the bandwidth of the filter.

C. Flux Controller

In order to speed up the rotor-flux dynamics, a proportional flux controller with a feedforward term is applied. A voltage-feedback field-weakening algorithm is integrated into the flux controller for enabling high-speed operation. The reference for the flux-producing current component is

$$i'_{\text{sd,ref}} = \frac{\psi_{R,\text{ref}}}{L_M} + K_f(\psi_{R,\text{ref}} - \hat{\psi}_R) + I_u \quad (29)$$

$$\text{with the limitation } -\frac{i_{s,\text{max}}}{\sqrt{2}} \leq i'_{\text{sd,ref}} \leq \frac{i_{s,\text{max}}}{\sqrt{2}}$$

where $K_f = \alpha_f/(\gamma R_R) - 1/L_M$ is the gain, α_f is the closed-loop bandwidth, and $i_{s,\text{max}}$ is the maximum stator current. The field-weakening term similar to [17] is applied,

$$I_u = K_u \int \underbrace{(u_{s,\text{max}}^2 - u_{s,\text{ref}}^2)}_{\varepsilon_u} dt \quad (30)$$

$$\text{with the limitation } I_u \leq 0$$

where $K_u = \hat{\psi}_R R_R / (L_\sigma u_{s,\text{max}})^2$ is the gain and $u_{s,\text{max}}$ is the maximum voltage corresponding to the linear modulation region [18]. The term I_u is non-zero only at high speeds. The torque-producing current component is evaluated as

$$i'_{\text{sq,ref}} = \frac{T_{e,\text{ref}}}{\gamma \hat{\psi}_R} \quad (31)$$

In addition, limitations corresponding to the maximum current and the breakdown torque are applied.

IV. EXPERIMENTAL SETUP AND PARAMETERS

The performance of the proposed method is investigated by means of computer simulations and experiments in Section V. The experimental setup and the parameters are described in the following.

A. Experimental Setup

A 2.2-kW four-pole IM is used in the laboratory experiments. The rated values of the motor are given in Table I and the base values of the per-unit system in Table II. In all experiments, including no-load tests, the IM is fed by a frequency converter controlled by a dSPACE DS1103 PPC/DSP board. A servo motor is used as a loading machine. The total moment of inertia of the experimental setup is 0.015 kgm². The speed is measured using an incremental encoder for monitoring purposes. A Voltech PM6000 power analyzer is applied in steady-state loss measurements.

The phase currents are measured using LEM LA 55-P/SP1 transducers, and the sampling is synchronized to the pulse-width modulation. The stator voltages are evaluated from the

TABLE I
RATED VALUES OF 2.2-KW 4-POLE 400-V IM

Power P_N	2.2 kW
Line-to-line voltage U_N	400 V (rms)
Current I_N	5 A (rms)
Frequency f_N	50 Hz
Rotation speed n_N	1436 r/min
Shaft torque T_N	14.6 Nm

TABLE II
BASE VALUES OF PER-UNIT SYSTEM

Voltage u_B	$\sqrt{2/3}U_N$
Current i_B	$\sqrt{2}I_N$
Frequency f_B	f_N
Angular frequency ω_B	$2\pi f_N$
Flux linkage ψ_B	u_B/ω_B
Impedance Z_B	u_B/i_B
Inductance L_B	Z_B/ω_B

measured dc-link voltage and the switching states. The effect of inverter nonlinearities on the stator voltage is substantial at low speeds. Therefore, the most significant inverter nonlinearities, i.e. the dead-time effect and power device voltage drops, are compensated for. Using phase a as an example, a compensated duty cycle is evaluated as [16]

$$d_a = d_{a,\text{ref}} + \frac{2d_\delta}{\pi} \arctan\left(\frac{i_a}{i_\delta}\right) \quad (32)$$

where $d_{a,\text{ref}}$ is the ideal duty cycle obtained from the current controller and i_a is the phase current. The parameter $d_\delta = 0.011$ p.u. takes into account both the dead-time effect and the threshold voltage of the power devices. The shape of the arctan function is determined by the parameter $i_\delta = 0.21$ p.u. The current-feedforward compensation method in (32) corresponds to the method in [19], [20], except that the signum functions were replaced with the arctan functions in order to improve the performance in the vicinity of current zero crossings.

Unless otherwise noted, the maximum stator current is $i_{s,\text{max}} = 1.5$ p.u. The sampling period of the pulse-width modulator, current controller and flux observer is 200 μs , and the sampling period of the rest of the control system is 1 ms. The flux-reference filter bandwidth $\alpha_{\text{lpf}} = 0.06$ p.u. and the flux-control bandwidth $\alpha_f = 0.06$ p.u. Furthermore, the bandwidth of 0.06 p.u. is used for the speed control. The minimum and maximum values of the flux reference are $\psi_{R,\text{min}} = 0.2$ p.u. and $\psi_{R,\text{max}} = 1.2$ p.u., respectively. The per-unit observer gains equal to [16] were applied in the experiments.

B. Parameter Identification

Per-unit motor parameters used in the simulations and experiments are given in Table III. The identification procedure for the parameters of the stator inductance function (5) and the core-loss conductance function (8) is described in the following.

The stator resistance R_s was measured in advance by means of a dc test. No-load tests were performed to obtain the parameters used in the stator-inductance function (5) and in the core-loss conductance function (8). The stator voltage

TABLE III
PER-UNIT MOTOR PARAMETERS

Stator resistance R_s	0.065
Rotor resistance R_R	0.040
Leakage inductance L_σ	0.17
Stator inductance function	
Unsaturated inductance L_u	2.31
Constant β	0.87
Constant S	7
Core-loss conductance function	
Constant Λ_{Hy}	0.015
Constant G_{Ft}	0

and current were measured at four different stator frequencies (0.3, 0.5, 0.7, and 0.8 p.u.) and at six different voltage levels (approximately corresponding to the stator-flux values between 0.2 p.u. and 1.2 p.u.). At each operating point, the voltage $\mathbf{u}_{Fe} = \mathbf{u}_s - R_s \mathbf{i}_s$ and the stator flux $\psi_s = -\mathbf{J} \mathbf{u}_{Fe} / \omega_s$ were evaluated.

The parameters of the inductance function (5) were obtained by minimizing

$$J_L(L_u, \beta, S) = \sum_{n=1}^N \left[i'_{s,n} - \frac{\psi_{s,n}}{L_M(\psi_{s,n})} \right]^2 \quad (33)$$

where $i'_s = \mathbf{i}_s^T \psi_s / \psi_s$ is the component of the stator current in the direction of the stator-flux vector and N is the total number of operating points. As a result, the parameters S , L_u , and β given in Table III were obtained. The inductances $\psi_{s,n} / i'_{s,n}$ obtained from the measurement data and the fitted inductance (5) are shown in Fig. 2. It can be seen that the function (5) fits very well to the data.

The parameters of the conductance function (8) were obtained by minimizing

$$J_G(G_{Ft}, \Lambda_{Hy}) = \sum_{n=1}^N [i_{Fe,n} - G_{Fe}(\omega_{s,n}) \cdot u_{Fe,n}]^2 \quad (34)$$

where $i_{Fe} = \mathbf{i}_s^T \mathbf{u}_{Fe} / u_{Fe}$. At the frequencies used in the no-load tests, the core losses of this machine consist mainly of the hysteresis losses; based on the fitting, the core-loss parameters Λ_{Hy} and G_{Ft} given in Table III were obtained. At higher frequencies, the influence of G_{Ft} would probably become more significant. In the control system, the maximum value of the conductance function G_{Fe} is limited to 0.2 p.u. The core-loss conductances $i_{Fe,n} / u_{Fe,n}$ obtained from the measured data and the fitted conductance (8) are shown in Fig. 3. It can be seen that the measured values of the core-loss conductance depend on the flux level in addition to the stator frequency.

Alternatively, if a priori information of the motor is available, the core-loss parameters could be calculated as

$$\Lambda_{Hy} = \frac{k_{Hy} P_{FeN}}{\omega_{sN} \psi_{sN}^2}, \quad G_{Ft} = \frac{(1 - k_{Hy}) P_{FeN}}{\omega_{sN}^2 \psi_{sN}^2} \quad (35)$$

where P_{FeN} are the rated core losses and k_{Hy} is the ratio between the hysteresis losses and the total core losses in the rated operating point.³ The rated stator flux is ψ_{sN} and the rated stator angular frequency is ω_{sN} .

³Applying P_{FeN} and k_{Hy} provided in [18] for the same IM, the parameters $\Lambda_{Hy} = 0.022$ p.u. and $G_{Ft} = 0.007$ p.u. are obtained.

V. RESULTS

A. Parameter Sensitivity

In order to investigate the parameter sensitivity of the core-loss model, computer simulations were carried out in MATLAB/Simulink environment. The IM was modeled as described in Section II, the control system was modeled according to Section III, and the parameters in Table III were used.

The core-loss model is included in the observer. Inaccurate parameters cause errors in the estimates of the rotor-flux magnitude and position and, thus, in the estimated torque. As an example, at the speed 0.5 p.u. and torque 30% of the rated torque, the torque error is 4% if the core losses are omitted in the control system. If the estimated value of Λ_{Hy} is twice its actual value, the corresponding torque error is 3%. The relative torque error decreases as the load increases. For instance, at the speed 0.5 p.u. and torque equal to the rated torque, the error in the estimated torque is 2% if the core losses are omitted.

The core-loss model affects the evaluation of the optimum flux level in the loss control directly. As an example, at the speed 0.5 p.u. and torque 30% of the rated torque, the flux level increases 9% if the core losses are omitted in the control system. This relatively large increase in the flux level causes losses to increase only 0.2%.

B. Experimental Results

The performance of the proposed method was investigated experimentally by means of dynamic test sequences and steady-state loss measurements.

1) *Dynamic Experiments:* In Fig. 6, the speed reference was stepped from 0 to 0.5 p.u. at $t = 1$ s and back to 0 at $t = 4$ s. A rated load torque step was applied at $t = 2$ s and removed at $t = 3$ s. Fig. 6(a) shows the result of the constant-flux control and Fig. 6(b) is the result of proposed loss-minimizing flux control. It can be seen that the flux estimate follows the loss-minimizing flux reference. The proposed method reduces both the steady-state rotor flux and stator current in this case.

Changes in the speed reference or load torque result in a varying torque reference, which in turn causes changes in the loss-minimizing rotor flux reference. The rate of change of the rotor flux reference is restricted by the bandwidth α_{lpf} . The changes in the actual rotor flux are slower due to the rotor time constant. A low rotor flux level is used at low torques, and increasing the torque takes more time when the loss-minimizing flux control is used than in constant-flux operation, although the current control uses the maximum current when large changes in the flux are required. Therefore, the acceleration in Fig. 6(b) is slower than that in Fig. 6(a), and the speed change after the load torque step is larger. However, the dynamic performance of the proposed method is acceptable for many applications. For higher dynamic response requirements, the minimum-flux limit can be raised.

Fig. 7 shows an acceleration from standstill to a speed of 1.5 p.u. and a speed reversal. During the transients, the flux is reduced by the field-weakening term (30) since all the available voltage is in use. For a fast reduction of the flux level, the d-axis current becomes negative at about $t = 1.16$

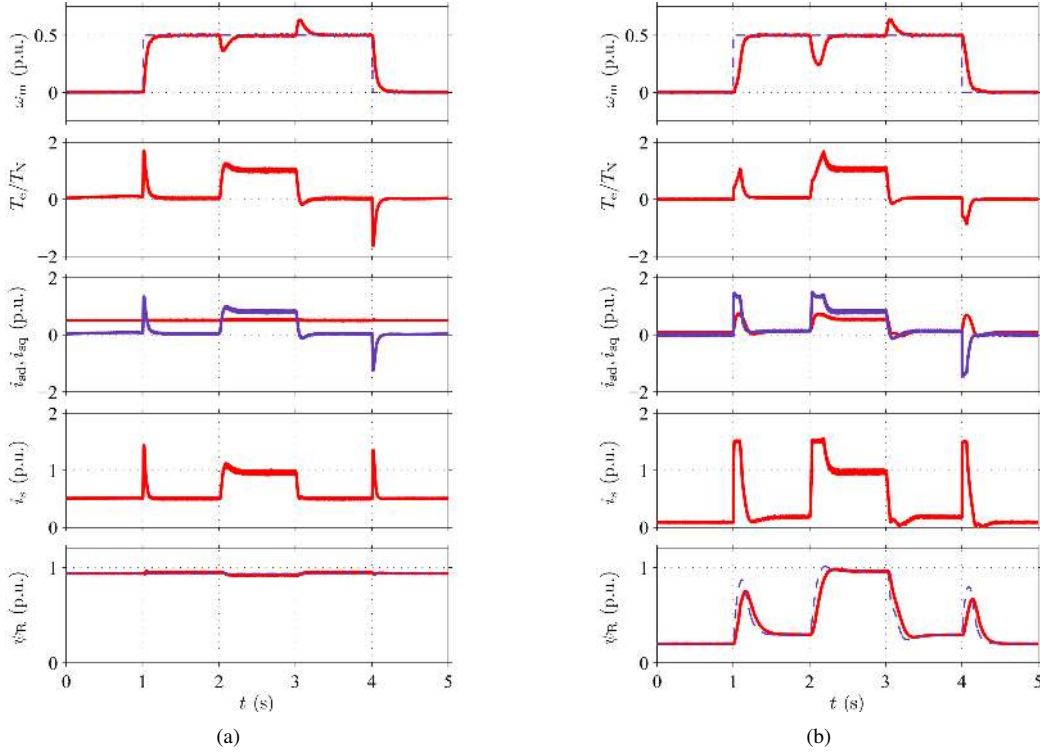


Fig. 6. Experimental results showing speed reference steps and a load torque step: (a) constant-flux control; (b) loss-minimizing flux control. The uppermost subplot shows the speed reference and the measured speed, the second subplot shows the estimated torque, the third subplot shows the stator current components, the fourth subplot shows the stator current magnitude and the last subplot shows the rotor flux reference (dashed) and the estimated rotor flux (solid).

s in accordance with the limits in (29). As steady state is reached, the flux follows the flux reference given by the loss-minimizing algorithm, and the losses are minimized.

In Fig. 8, operation at zero speed is shown. A rated load torque step is applied at $t = 1.5$ s, and a negative torque step twice the rated torque is applied at $t = 2.5$ s. The load is removed at $t = 3.5$ s. As discussed in more detail in [16], speed-sensorless operation at zero speed is possible since (i) the inverter nonlinearities are compensated for, (ii) observer gains are properly selected, and (iii) stator-resistance adaptation together with good inductance estimates is applied. Even if the initial flux level is low at $t = 1.5$ s, the system tolerates the load torque step without problems.

2) *Steady-State Losses*: Experiments were carried out to compare the steady-state losses between the proposed method and constant-flux control. The core losses were omitted in the flux observer in constant-flux control.

A Voltech PM6000 power analyzer was used for measuring the input power to the IM, the mechanical output power was calculated from the measured speed and the shaft torque (measured with a HBM T10F torque flange), and the total losses of the IM in steady state were determined. In order to exclude the influence of temperature changes, a cooling time was allowed between the experiments, and the stator resistance estimate was followed.

The fundamental component of the stator voltage was also recorded with the power analyzer. The maximum available output voltage of the converter was limited below 1 p.u., since the diode rectifier of the frequency converter was connected

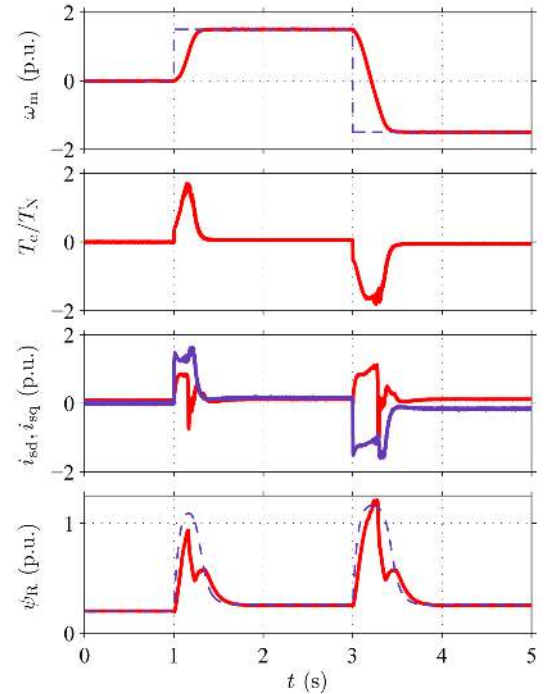


Fig. 7. Experimental results showing operation in the field-weakening region.

to a 380-V 50-Hz supply (while the base values are based on the rated values of the 400-V IM). Furthermore, the linear modulation region in steady state and a minimum pulse-width limitation were applied.

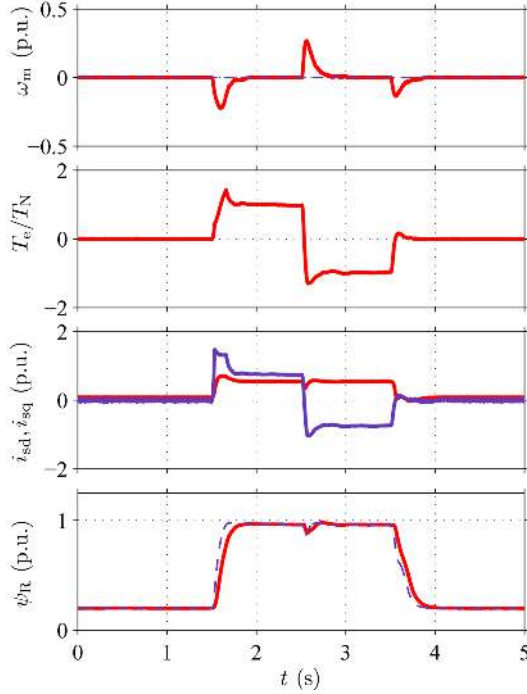


Fig. 8. Experimental results showing load torque steps at zero speed.

Fig. 9 shows the measured total losses of the IM and the stator voltage as a function of the measured shaft torque. Measurements were carried out at the speeds of 0.5 p.u. and 1.0 p.u. The results show that the proposed method significantly reduces the losses in steady state at low loads. At the speed of 0.5 p.u., the losses are reduced not only in the low-torque region but also at torque levels above the rated torque. The improvement at high torque levels is achieved by applying a flux higher than the rated flux, in accordance with Fig. 4.

The maximum achievable flux level is limited at higher speeds by the maximum stator voltage.⁴ It can be seen in Fig. 9 that, at the speed of 1.0 p.u., the loss-minimizing flux level cannot be applied if the torque is more than approximately half the rated torque. In this case, the flux level is (automatically) determined by the voltage-feedback field-weakening algorithm (30).

Fig. 10 shows the measured losses as a function of the rotor flux estimate. Four different shaft torque values were applied while the speed was kept at 0.5 p.u. It can be seen that measured losses depend on the rotor flux, and that losses can be minimized by suitably selecting the flux level. Furthermore, the loss-minimizing flux level was calculated for each torque using (27). It can be seen that the flux from (27) agrees well with the actual loss-minimizing flux.

3) *S5 Duty Cycle*: Experiments were also carried out in intermittent periodic duty with acceleration and electric braking (IEC duty type S5 60%, $J_M = 0.0069 \text{ kgm}^2$, $J_{\text{ext}} = 0.0086 \text{ kgm}^2$). During the operation time, the load was 30% of the

⁴The maximum achievable stator voltage decreases slightly with the increasing torque, since the dc-link voltage decreases with the increasing load and there are load-dependent voltage drops in the inverter and cables.

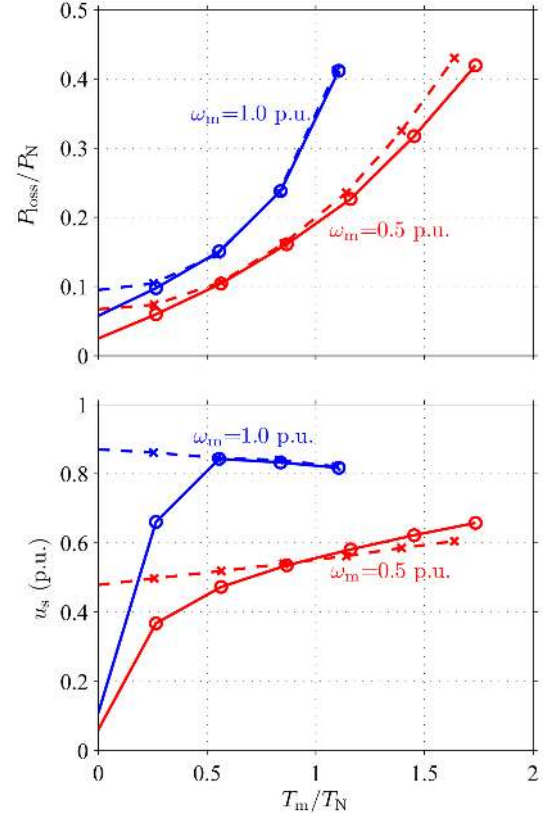


Fig. 9. Experimental results showing the total losses of the motor and the stator voltage as a function of the measured torque at speeds of 0.5 p.u. and 1.0 p.u. The first subplot shows the losses and the second subplot shows the fundamental component of the stator voltage. Solid lines marked with circles are the results obtained with the proposed method and dashed lines marked with stars are the results with constant-flux control.

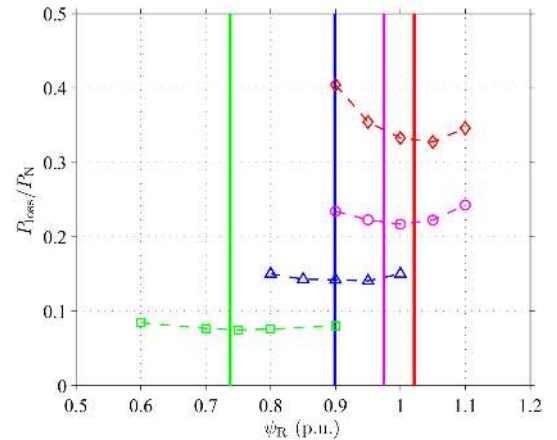


Fig. 10. Measured losses (markers) as a function of the rotor flux and theoretical optimal rotor flux values (vertical lines). The speed is 0.5 p.u. The torque is $0.38T_N$ (squares), $0.77T_N$ (triangles), $1.14T_N$ (circles) and $1.49T_N$ (diamonds).

rated torque, and the speed was 0.8 p.u. The maximum stator current was $i_{s,\text{max}} = 2.0 \text{ p.u.}$ Fig. 11 shows an example of the measured results for the cycle duration of 3 s.

Both the loss-minimizing algorithm and the constant-flux control were applied. The mean value of the input power was calculated off-line using the phase currents, dc-link voltage,

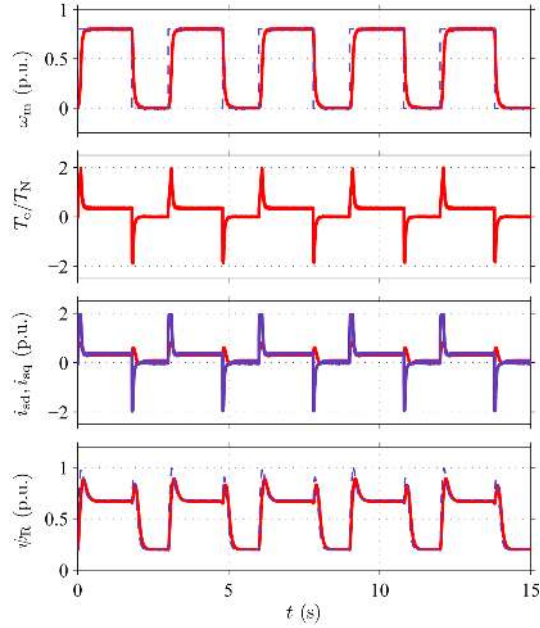


Fig. 11. S5 duty cycles.

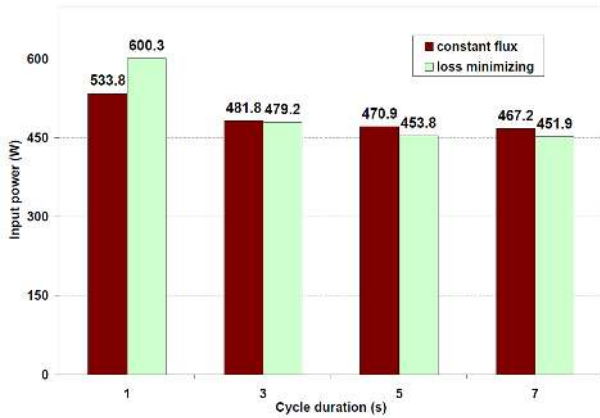
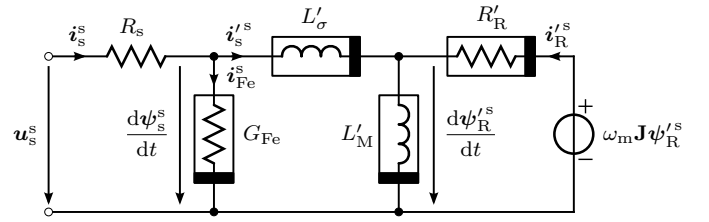


Fig. 12. Input power measurement of S5 duty cycles.

and switching states, which were captured with the DS1103 board. Fig. 12 shows the results for different cycle durations between 1 s and 7 s. It can be seen that loss-minimizing flux optimization leads to lower losses than the constant-flux approach if the cycle duration is long enough. In the case of the shortest cycle durations, the current required for changing the flux in accelerations and decelerations contributes to the losses so much that the constant-flux operation becomes more beneficial.

VI. CONCLUSION

This paper proposed a loss-minimizing flux control method for the IM drive. The magnetic saturation as well as the hysteresis and eddy-current losses are included in the loss minimization, flux estimation, and sensorless control of the IM. The proposed system provides smooth transitions between the loss-minimizing region at lower speeds and the voltage-feedback field-weakening region at higher speeds. Based on

Fig. 13. Inverse- Γ model in stator coordinates.

the simulation studies of a 2.2-kW IM drive system, the loss-minimizing algorithm is not very sensitive to errors in core-loss model parameters. The inclusion of the core-loss model in the flux observer notably improves the accuracy of the torque production.

The experimental results show that the dynamic performance of the method is acceptable. The losses in steady state are significantly reduced in a wide torque range, as compared to the losses in the constant-flux approach. It was also experimentally demonstrated that the actual loss minimum is achieved for all practical purposes. In intermittent periodic duty, the proposed method reduces the losses if the cycle duration is long enough. In the case of the shortest cycle durations, the constant-flux operation becomes more beneficial.

APPENDIX INVERSE- Γ MODEL

In the case of rotor-flux orientation control, the inverse- Γ model shown in Fig. 13 is typically preferred in the design and implementation of the control algorithms. The parameters and variables of the Γ model can be transformed to those of the inverse- Γ model using the coupling factor

$$\gamma = \frac{L_M}{L_M + L_\sigma} = \frac{L_u}{L_u + L_\sigma + L_\sigma(\beta\psi_s)^S} \quad (36)$$

as follows:

$$L'_\sigma = \gamma L_\sigma \quad L'_M = \gamma L_M \quad R'_R = \gamma^2 R_R \quad (37)$$

When this transformation is used, the models are mathematically equivalent in steady state (and in transients as well if the magnetics are linear). It can be seen that due to the magnetic saturation, the equivalent inverse- Γ model parameters depend on the stator flux. The rotor flux can be transformed to inverse- Γ flux as $\psi'_R = \gamma\psi_R$.

ACKNOWLEDGMENT

This paper is dedicated to the memory of Prof. Jorma Luomi, who passed away in December 2011 after a short battle against cancer.

REFERENCES

- [1] S. N. Vukosavic and E. Levi, "Robust DSP-based efficiency optimization of a variable speed induction motor drive," *IEEE Trans. Ind. Electron.*, vol. 50, no. 3, pp. 560–570, June 2003.
- [2] A. M. Bazzi and P. T. Krein, "Review of methods for real-time loss minimization in induction machines," *IEEE Trans. Ind. Appl.*, vol. 46, no. 6, pp. 2319–2328, Nov./Dec. 2010.

- [3] G. O. Garcia, J. C. Mendes Luís, R. M. Stephan, and E. H. Watanabe, "An efficient controller for an adjustable speed induction motor drive," *IEEE Trans. Ind. Electron.*, vol. 41, no. 5, pp. 533–539, Oct. 1994.
- [4] F. Abrahamsen, F. Blaabjerg, J. K. Pedersen, P. Z. Grabowski, and P. Thogesen, "On the energy optimized control of standard and high-efficiency induction motors in CT and HVAC applications," *IEEE Trans. Ind. Appl.*, vol. 34, no. 4, pp. 822–831, July-Aug. 1998.
- [5] S. Lim and K. Nam, "Loss-minimising control scheme for induction motors," *IEE Proc. Electr. Power Appl.*, vol. 151, no. 4, pp. 385–397, July 2004.
- [6] I. Kioskeridis and N. Margaris, "Loss minimization in scalar-controlled induction motor drives with search controllers," *IEEE Trans. Power Electron.*, vol. 11, no. 2, pp. 213–220, Mar. 1996.
- [7] T. R. Obermann, Z. D. Hurst, B. F. Bradley, and R. D. Lorenz, "Deadbeat-direct torque & flux control motor drive using a single control law to minimize motor losses," in *Proc. ICEMS'10*, Incheon, Korea (South), Oct. 2010, pp. 742–747.
- [8] M. Ranta, M. Hinkkanen, E. Dlala, A.-K. Repo, and J. Luomi, "Inclusion of hysteresis and eddy current losses in dynamic induction machine models," in *Proc. IEEE IEMDC'09*, Miami, FL, May 2009, pp. 1387–1392.
- [9] G. R. Slemon, "Modelling of induction machines for electric drives," *IEEE Trans. Ind. Appl.*, vol. 25, no. 6, pp. 1126–1131, Nov/Dec. 1989.
- [10] T. Tuovinen, M. Hinkkanen, and J. Luomi, "Modeling of saturation due to main and leakage flux interaction in induction machines," *IEEE Trans. Ind. Appl.*, vol. 46, no. 3, pp. 937–945, May/June 2010.
- [11] M. Hinkkanen, A.-K. Repo, and J. Luomi, "Influence of magnetic saturation on induction motor model selection," in *Proc. IECM'06*, Chania, Greece, Sept. 2006, CD-ROM.
- [12] H. C. J. de Jong, "Saturation in electrical machines," in *Proc. IECM'80*, vol. 3, Athens, Greece, Sept. 1980, pp. 1545–1552.
- [13] D. W. Novotny, S. A. Naser, B. Jeftenic, and D. Maly, "Frequency dependence of time harmonic losses in induction machines," in *Proc. IECM'90*, vol. 1, Raleigh, NC, Aug. 1990, pp. 233–238.
- [14] G. C. Verghese and S. R. Sanders, "Observers for flux estimation in induction machines," *IEEE Trans. Ind. Electron.*, vol. 35, no. 1, pp. 85–94, Feb. 1988.
- [15] S. Sangwongwanich, U. Nittayatareekul, and P. Magyar, "Direct speed estimation based on back EMF of induction motors – its equivalent MRAS representation and stability analysis," in *Proc. EPE'03*, Toulouse, France, Sept. 2003, CD-ROM.
- [16] M. Hinkkanen, L. Harnefors, and J. Luomi, "Reduced-order flux observers with stator-resistance adaptation for speed-sensorless induction motor drives," *IEEE Trans. Power Electron.*, vol. 25, no. 5, pp. 1173–1183, May 2010.
- [17] L. Harnefors, "Design and analysis of general rotor-flux-oriented vector control systems," *IEEE Trans. Ind. Electron.*, vol. 48, no. 2, pp. 383–390, Apr. 2001.
- [18] M. Hinkkanen and J. Luomi, "Braking scheme for vector-controlled induction motor drives equipped with diode rectifier without braking resistor," *IEEE Trans. Ind. Appl.*, vol. 42, no. 5, pp. 1257–1263, Sept./Oct. 2006.
- [19] J. K. Pedersen, F. Blaabjerg, J. W. Jensen, and P. Thogersen, "An ideal PWM-VSI inverter with feedforward and feedback compensation," in *Proc. EPE'93*, vol. 4, Brighton, U.K., Sept. 1993, pp. 312–318.
- [20] J.-W. Choi and S.-K. Sul, "Inverter output voltage synthesis using novel dead time compensation," *IEEE Trans. Power Electron.*, vol. 11, no. 2, pp. 221–227, Mar. 1996.



Zengcai Qu received the B.Sc. in electrical engineering and automation in Shanghai Jiao Tong University, Shanghai, China in 2007, and M.Sc. degree in Space Science and Technology from Lulea University of Technology, Kiruna, Sweden and Helsinki University of Technology, Espoo, Finland in 2009.

Since 2009, he is currently working towards the Ph.D. degree in Aalto University, Espoo, Finland. His research interest is efficiency control of electric drives.



Mikaela Ranta Mikaela Ranta received the M.Sc.(Eng.) degree from Helsinki University of Technology, Espoo, Finland, in 2006.

Since 2006, she has been with Aalto University. She is currently a Research Scientist in the Aalto University, School of Electrical Engineering, Espoo, Finland. Her main research interest is the modeling of electric machines.



Marko Hinkkanen (M'06) received the M.Sc.(Eng.) and D.Sc.(Tech.) degrees from the Helsinki University of Technology, Espoo, Finland, in 2000 and 2004, respectively.

Since 2000, he has been with the Helsinki University of Technology (part of Aalto University since 2010). He is currently an Adjunct Professor in the Aalto University School of Electrical Engineering, Espoo, Finland. His research interests include electric drives and electric machines.



Jorma Luomi (M'92) received the M.Sc.(Eng.) and D.Sc.(Tech.) degrees from the Helsinki University of Technology, Espoo, Finland, in 1977 and 1984, respectively.

He joined the Helsinki University of Technology in 1980, and from 1991 to 1998, he was a Professor at Chalmers University of Technology, Göteborg, Sweden. Since 1998, he was a Professor in the Helsinki University of Technology (part of Aalto University since 2010), Espoo, Finland. His research interests included electric drives, electric machines,

and numerical analysis of electromagnetic fields.

Prof. Luomi passed away in December 2011.